

1-1-2000

Novel Charge-Transfer Materials via Cocrystallization of Planar Aromatic Donors and Spherical Polyoxometalate Acceptors

P. Le Maguères
University of Houston

S. M. Hubig
University of Houston

Sergey V. Lindeman
Marquette University, sergey.lindeman@marquette.edu

P. Peya
University of Houston

Jay K. Kochi
University of Houston

Accepted version. *Journal of the American Chemical Society*, Vol. 122, No. 41 (2000): 10073-10082.

DOI. © 2000 American Chemical Society. Used with permission.

Sergey V. Lindeman was affiliated with the University of Houston at the time of publication.

Marquette University

e-Publications@Marquette

Chemistry Faculty Research and Publications/College of Arts and Sciences

This paper is NOT THE PUBLISHED VERSION; but the author's final, peer-reviewed manuscript. The published version may be accessed by following the link in the citation below.

Journal of the American Chemical Society, Vol. 122, No. 41 (2000): 10073-10082. [DOI](#). This article is © American Chemical Society and permission has been granted for this version to appear in [e-Publications@Marquette](#). American Chemical Society does not grant permission for this article to be further copied/distributed or hosted elsewhere without the express permission from American Chemical Society.

Novel Charge-Transfer Materials via Cocrystallization of Planar Aromatic Donors and Spherical Polyoxometalate Acceptors

P. Le Maguerès

Department of Chemistry, University of Houston, Houston, Texas

S. M. Hubig

Department of Chemistry, University of Houston, Houston, Texas

S. V. Lindeman

Department of Chemistry, University of Houston, Houston, Texas

P. Veya

Department of Chemistry, University of Houston, Houston, Texas

J. K. Kochi

Department of Chemistry, University of Houston, Houston, Texas

Abstract

Spherical polyoxometalates (POMs) such as $M_6O_{19}^{2-}$ and $SiM_{12}O_{40}^{4-}$ (with M = Mo or W) and planar arene donors (anthracenes and pyrenes) can be cocrystallized (despite their structural incompatibility) by attaching a cationic

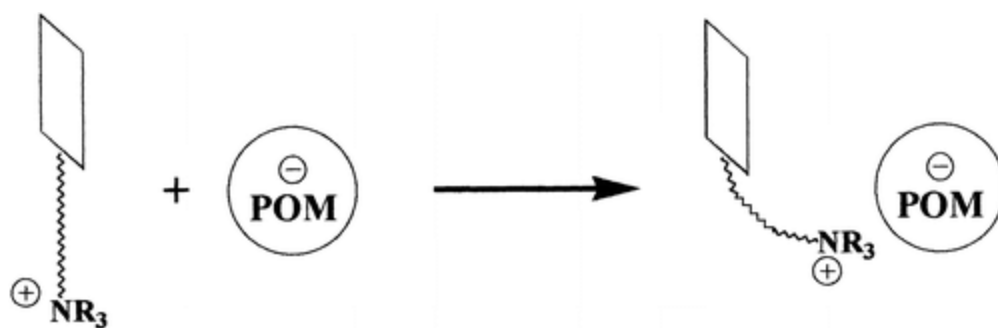
“anchor” onto the arene which then clings to the POM anion by Coulombic forces. As a result, novel charge-transfer (CT) salts are prepared from arene donors and Lindqvist-type $[M_6O_{19}]^{2-}$ and Keggin-type $[SiM_{12}O_{40}]^{4-}$ acceptors with overall 2:1 and 4:1 stoichiometry, respectively. The CT character of the dark-colored (yellow to red) crystalline materials is confirmed by the linear Mulliken correlation between the CT transition energies and the reduction potentials of the POM acceptors, as well as by the transient (diffuse reflectance) absorption spectra (upon picosecond laser excitation) of anthracene or pyrene cation radicals (in monomeric and π -dimeric forms). X-ray crystallographic studies reveal a unique “dimeric” arrangement of the cofacially oriented arene couples which show contact points with the oxygen surface of the POMs that vary with distance, depending on the POM/arene combination. Moreover, the combination of X-ray crystallographic and spectroscopic techniques results in the observation of a logical structure/property relationship — the shorter the distance between the POM surface and the arene nucleus, the darker is the color of the CT crystal and the faster is the decay of the laser-excited charge-transfer state (due to back-electron transfer).

Introduction

Metal oxide clusters or polyoxometalates (POMs) have attracted great attention in recent years due to their versatility and utility in catalysis (e.g., photochemical dehydrogenations of organic substrates), medicine (e.g., anti-viral and anti-tumor drugs), and material sciences.¹ This broad range of applications is based on (i) the ability of POMs to act as electron reservoirs² and (ii) the extreme variability of their molecular properties, including size, shape, charge, charge density, redox potential, acidity, solubility, etc.^{1,3} Of particular interest is the use of POMs as electron-accepting moieties in charge-transfer materials that are prepared by cocrystallization with organic donors including substituted amides,⁴ aromatic amines,⁵ or electron-rich substrates such as tetrathiafulvenes or decamethylferrocene.⁶ Most importantly, the donor/acceptor interactions in such charge-transfer materials, which affect the ferromagnetic, nonlinear optical, and conducting properties, are critically controlled by the size and shape of the POMs as well as by their reduction potentials, which are readily tuned by varying the metal centers.

The cocrystallization of the bulky spherical polyoxometalates with planar aromatic compounds represents an enormous experimental challenge.⁷ Certainly, the donor/acceptor interactions between the “hard” POM acceptors and the “soft” aromatic (π -) donors are too weak to overcome the structural incompatibility of the two components. On the other hand, there are a few examples of charge-transfer crystals with POMs that are stabilized by hydrogen bonding,⁴ and the majority of POM cocrystals with organic donors are based on Coulombic forces in ion pairs consisting of (partially or fully) oxidized donors and reduced POMs.⁶

We have recently shown that Coulombic forces can also be utilized to prepare charge-transfer crystals with less electron-rich donors which are not oxidized to the cation radical state.⁸ Thus, a positively charged substituent (e.g., ammonium) attached to the aromatic donor via a flexible polymethylene chain is used as a cationic anchor that clings to the anionic polyoxometalate, as illustrated in Scheme 1.



Scheme 1

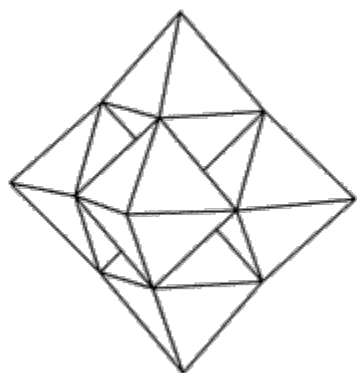
In this work, we will present a series of salts consisting of polyoxometalate anions and cationic arene donors, the stoichiometry of which is determined by the charges of the two components and their packing in the cocrystal. We will show that the new crystal engineering concept leads to a unique arrangement of the arene donors as cofacially oriented couples embedded between the spherical POM units. Moreover, the donor/acceptor interactions between the arene couples and the POM acceptor surface are found to vary significantly with the type of arene, the cationic anchor, and the POM unit chosen. The structural diversity of these new intensively colored materials is explored by X-ray crystallography, and the charge-transfer properties are examined by steady-state and time-resolved (diffuse reflectance) UV/vis spectroscopy.

Results

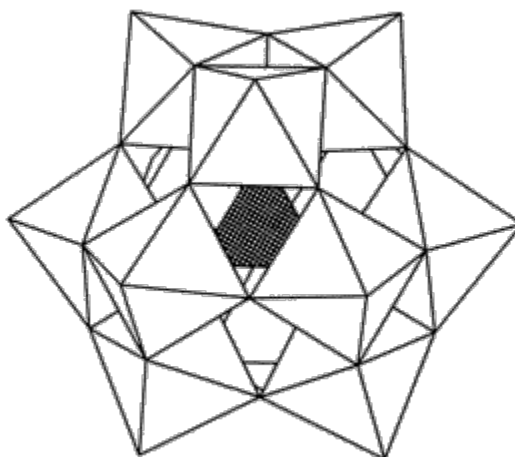
1. Preparation of Charge-Transfer Salts of Aromatic Donors with Polyoxometalates. 1. Synthesis of the Aromatic Donors. We prepared aromatic donors derived from anthracene or pyrene in which a cationic pyridinium or trialkylammonium substituent was remotely attached to the aromatic nucleus (ArH) via a flexible saturated hydrocarbon chain of variable length (see Chart 1). The various synthetic procedures are described in detail in the Experimental Section. Besides their different electron donicities, these aromatic donors exhibited various cationic anchors (viz., pyridinium or trialkylammonium) with different steric bulkiness (viz., trimethyl-, triethyl-, or tributylammonium groups) and had different lengths of the hydrocarbon chains (viz., one, three, or four methylene units).

2. Choice of the Polyoxometalate Acceptors. For this study, we chose the readily available Lindqvist-type $[M_6O_{19}]^{2-}$ and Keggin-type $[SiM_{12}O_{40}]^{4-}$ polyoxometalates⁹ with either molybdenum ($M = Mo$) or tungsten ($M = W$) as metal centers. In both of these structurally different classes of clusters, the modification of the metallic centers resulted in a significant variation of the reduction potentials by 400–500 mV (see Table 1). In addition, these POMs are commercially available as acids and can be easily converted to their tetrabutylammonium (Bu_4N^+) salts by direct metathesis with tetrabutylammonium bromide in aqueous solution (see the Experimental Section).

Polyoxometallate Structures

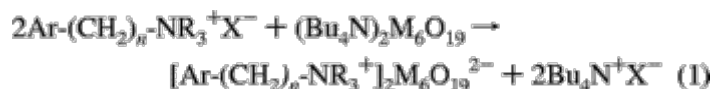


Lindqvist

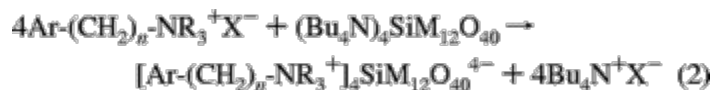


Keggin

3. Isolation of Crystalline Charge-Transfer Salts. The mixture of dilute acetonitrile solutions of the iodide or trifluoromethanesulfonate salts of $\text{Ar}-(\text{CH}_2)_n-\text{NR}_3^+$ and of $(\text{Bu}_4\text{N})_2[\text{M}_6\text{O}_{19}]$ ($\text{M} = \text{Mo}^{\text{VI}}, \text{W}^{\text{VI}}$) at 25 °C resulted in yellow solutions with a UV/vis spectrum that represented the sum of the absorption bands of the two components. However, upon the slow (1 or 2 days) evaporation of solvent, intensely colored crystals formed according to the 2:1 stoichiometry in eq 1, i.e.,



Similar treatment of dimethyl sulfoxide solutions of $\text{Ar}-(\text{CH}_2)_n-\text{NR}_3^+$ and $(\text{Bu}_4\text{N})_4[\text{SiM}_{12}\text{O}_{40}]$ ($\text{M} = \text{Mo}, \text{W}$) afforded strongly colored crystals of 4:1 salts, i.e.,



The color of these crystals faded immediately upon their dissolution in acetonitrile or dimethyl sulfoxide, and yellow solutions were obtained.¹⁰ Moreover, the UV/vis absorption spectra of solutions obtained from the colored crystals dissolved in dimethylformamide or dimethyl sulfoxide were identical to those of the mixture of both components prior to crystallization.¹¹

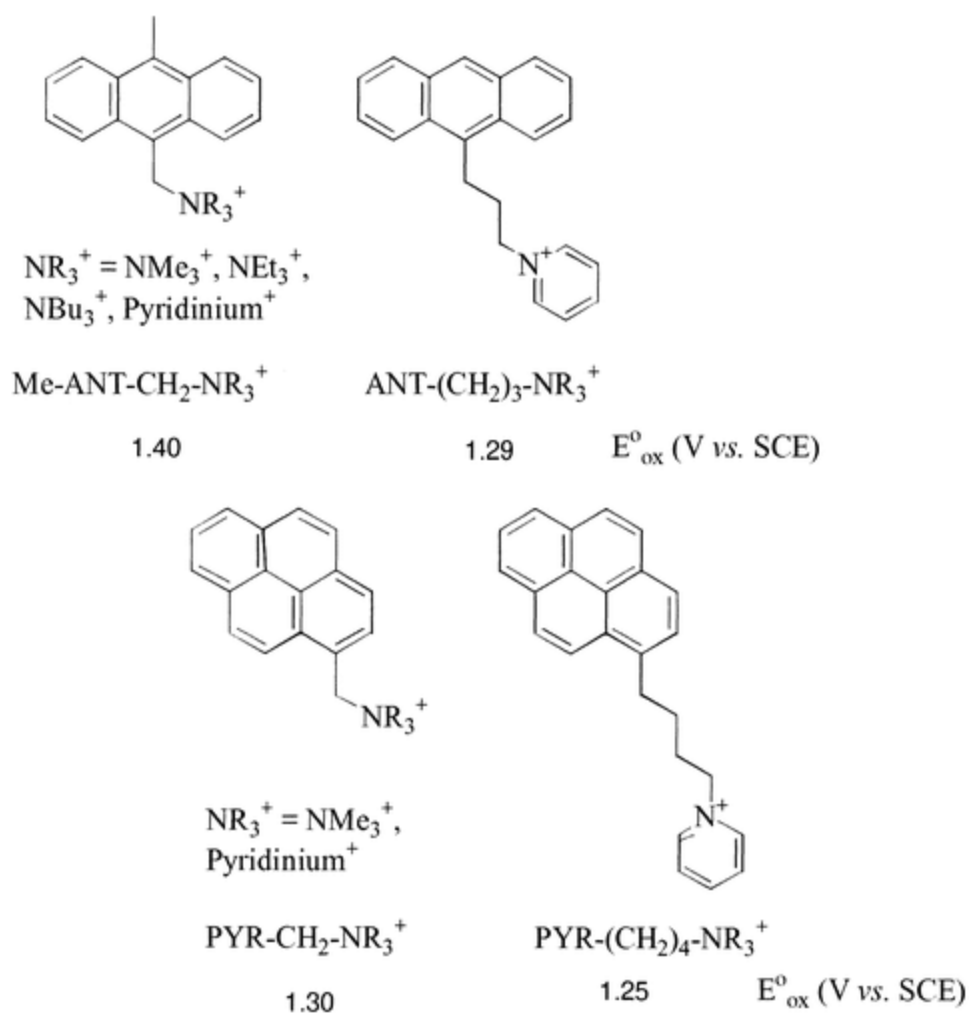


Chart 1

Table 1. Redox Potentials^a of the Bu₄N⁺ Salts of [M₆O₁₉]²⁻ and [SiM₁₂O₄₀]⁴⁻ (M = Mo^{VI}, W^{VI}) Acceptors

| | [W ₆ O ₁₉] ²⁻ | [Mo ₆ O ₁₉] ²⁻ | [SiW ₁₂ O ₄₀] ⁴⁻ | [SiMo ₁₂ O ₄₀] ⁴⁻ |
|--|---|--|--|---|
| E ^o _{red} (V vs SCE) | -0.96 | -0.44 | -0.75 | -0.36 |

^a In acetonitrile containing 5–7 mM POM and 100 mM Bu₄N⁺PF₆⁻ at 20 °C.

II. Spectroscopic Characterization of the Polyoxometalates Salts. Since the color of the various polyoxometalate salts was observed only in the solid state, UV/vis absorption spectra of the crystalline salts dispersed in alumina were obtained by the diffuse reflectance technique. The spectra exhibited broad, low-energy absorptions (tails) in addition to the local absorption bands of the components, rendering the determination of new absorption maxima difficult. Therefore, these new absorptions were described by the wavelength λ_0 at which the absorbance reached the baseline value.

1. Evidence for Charge-Transfer Interactions in the Polyoxometalates Salts. The 2:1 (physical) mixture of the iodide salt of Me-ANT-CH₂-Py⁺ (see Chart 1) and the (Bu₄N⁺) salt of either [Mo₆O₁₉]²⁻ or [W₆O₁₉]²⁻ in the solid state was transparent at wavelengths $\lambda > 500$ nm. In contrast, the crystalline 2:1 complex of Me-ANT-CH₂-Py⁺ with both polyoxometalates showed strong absorptions at $\lambda > 500$ nm

(see Figure 1A). Thus, the $[\text{Mo}_6\text{O}_{19}]^{2-}$ salt, which crystallized as bright-red crystals, showed a broad additional absorption that extended to $\lambda_o = 700$ nm, and the yellow-orange crystals of the isostructural $[\text{W}_6\text{O}_{19}]^{2-}$ salt showed a weak shoulder tailing to $\lambda_o = 550$ nm (see Table 2). The bathochromic shift with $\lambda_o(\text{W}_6\text{O}_{19}^{2-}) < \lambda_o(\text{Mo}_6\text{O}_{19}^{2-})$ corresponded to the order of the reduction potentials with $E^\circ_{\text{red}}(\text{W}_6\text{O}_{19}^{2-}) < E^\circ_{\text{red}}(\text{Mo}_6\text{O}_{19}^{2-})$ (compare Table 1).

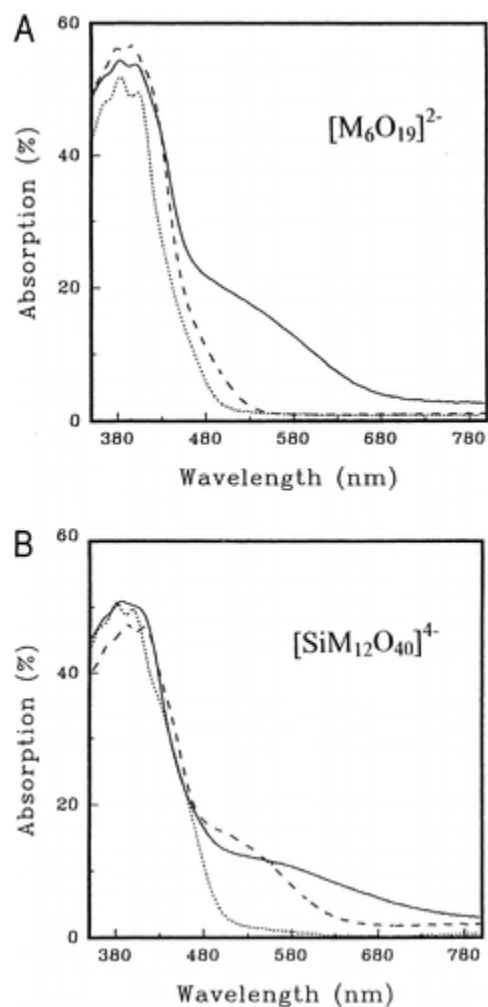
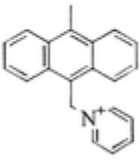


Figure 1 Diffuse reflectance spectra of the crystalline charge-transfer salts of Me-ANT-CH₂-Py⁺ donor with the POM acceptors: (A) $[\text{Mo}_6\text{O}_{19}]^{2-}$ (—) and $[\text{W}_6\text{O}_{19}]^{2-}$ (- - -) and (B) $[\text{SiMo}_{12}\text{O}_{40}]^{4-}$ (—) and $[\text{SiW}_{12}\text{O}_{40}]^{4-}$ (- - -). The dotted lines represent the diffuse reflectance spectra of the physical mixtures of the iodide salt of Me-ANT-CH₂-Py⁺ with (A) the Bu₄N⁺ salt of $[\text{W}_6\text{O}_{19}]^{2-}$ in a 2:1 ratio and (B) the Bu₄N⁺ salt of $[\text{SiW}_{12}\text{O}_{40}]^{4-}$ in a 4:1 ratio.

Table 2. Wavelengths (λ_o) at Which the Charge-Transfer Band Reaches the Baseline Value for the Charge-Transfer Salts of Me-ANT-CH₂-Py⁺ Donor with [M₆O₁₉]²⁻ and [SiM₁₂O₄₀]⁴⁻ (M = Mo^{VI}, W^{VI}) Acceptors

| | [W ₆ O ₁₉] ²⁻ | [Mo ₆ O ₁₉] ²⁻ | [SiW ₁₂ O ₄₀] ⁴⁻ | [SiMo ₁₂ O ₄₀] ⁴⁻ |
|---|---|--|--|---|
| | λ_o (nm) | λ_o (nm) | λ_o (nm) | λ_o (nm) |
|  | 550 (yellow-orange) | 720 (red) | 630 (orange) | 800 (red-brown) |

Similarly, the physical mixture of the iodide salt of Me-ANT-CH₂-Py⁺ with the (Bu₄N)⁺ salt of either [SiMo₁₂O₄₀]⁴⁻ or [SiW₁₂O₄₀]⁴⁻ did not show any absorption at $\lambda > 500$ nm. In contrast, the 4:1 isostructural complexes of Me-ANT-CH₂-Py⁺ with [SiMo₁₂O₄₀]⁴⁻ and [SiW₁₂O₄₀]⁴⁻ (dark-red and orange crystals, respectively) showed new absorptions extending up to $\lambda_o = 800$ nm and $\lambda_o = 640$ nm, respectively (see Figure 1B and Table 2). The red shift in λ_o accompanied an increase in the reduction potentials of the POM acceptors. Thus, in accord with Mulliken theory,¹² the new (visible) absorption bands were ascribed to charge-transfer transitions between the aromatic donors Me-ANT-CH₂-Py⁺ and the various POM acceptors, and the strongly colored crystals were identified as charge-transfer salts.¹³

2. Variation of the UV/Vis Absorption Spectra of Charge-Transfer Salts of Various Compositions and Structures. (a) Variation of the Cationic Anchor. When the same Lindqvist-type polyoxometalate [Mo₆O₁₉]²⁻ was mixed with a donor in which the pyridinium anchor was replaced by a trialkylammonium group NR₃⁺ (R = Me, Et, or Bu, see Chart 1), the color of the charge-transfer crystals changed significantly, and accordingly differences in the UV/vis spectra were observed.¹⁴ Thus, cocrystallization of the organic donors Me-ANT-CH₂-NMe₃⁺ and Me-ANT-CH₂-NEt₃⁺ with [Mo₆O₁₉]²⁻ led to dark-red crystals with broad (new) absorptions ($\lambda_o = 750$ nm) that were not present in the UV/vis spectra of the single components (see Figure 2 and Table 3). Interestingly, when the bulkier substituent (Bu₄N)⁺ was used as the cationic anchor of the electron donor, the color of the charge-transfer crystals obtained with the same POM [Mo₆O₁₉]²⁻ changed from red to orange. Accordingly, the UV/vis (diffuse reflectance) spectrum of [Me-ANT-CH₂-NBu₃]₂[Mo₆O₁₉] salt exhibited a charge-transfer absorption band that was blue-shifted by 100 nm relative to that observed with the charge-transfer crystals containing NMe₃⁺- and NEt₃⁺-substituted analogues (see Table 3).

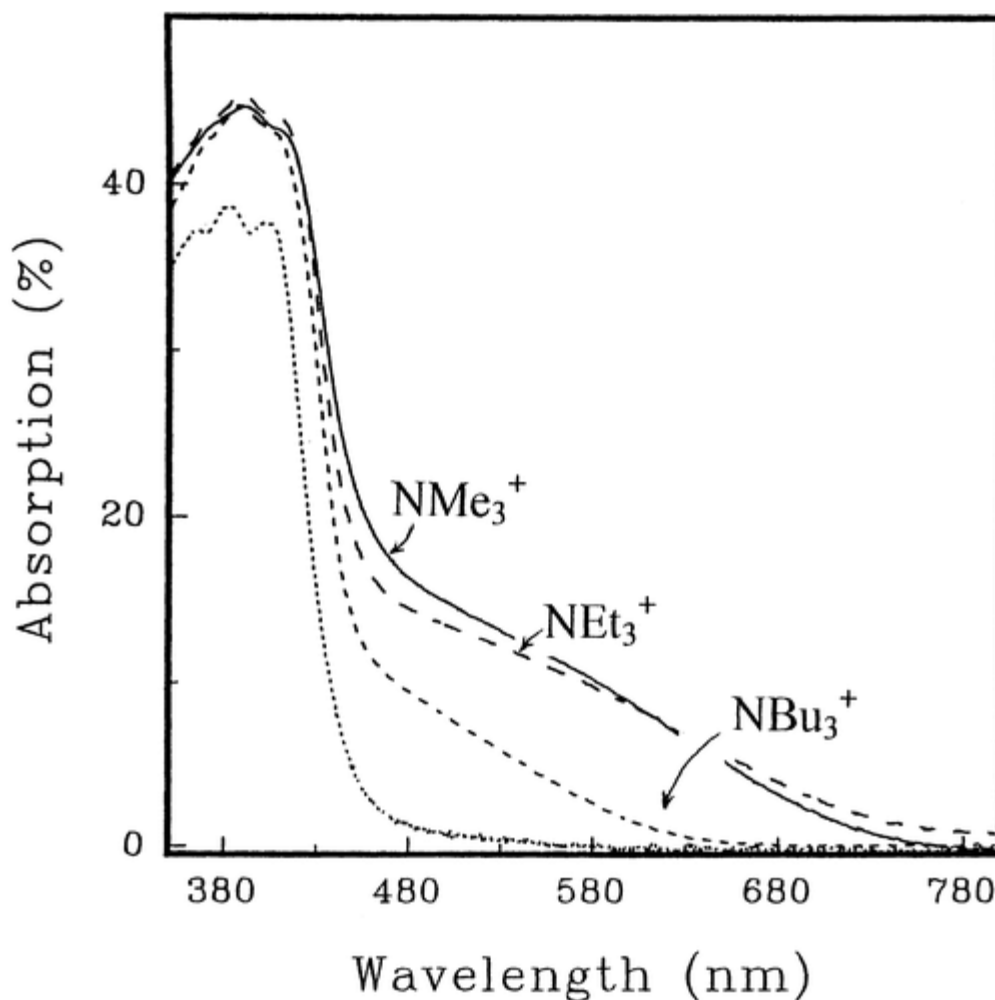
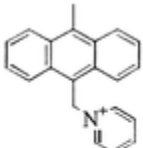
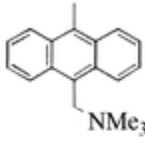
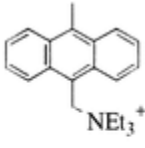
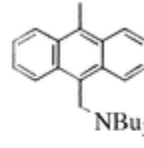


Figure 2 Diffuse reflectance spectra of the crystalline charge-transfer salts of $[\text{Mo}_6\text{O}_{19}]^{2-}$ acceptor with Me-ANT- $\text{CH}_2\text{-NR}_3^+$ donors: $\text{NR}_3^+ = \text{NMe}_3^+$ (—), NEt_3^+ (---), and NBu_3^+ (-.-). The dotted line represents the diffuse reflectance spectrum of the physical mixture of the Bu_4N^+ salt of $[\text{Mo}_6\text{O}_{19}]^{2-}$ with the iodide salt of Me-ANT- $\text{CH}_2\text{-NBu}_3^+$ in a 1:2 ratio.

Table 3. Wavelengths (λ_o) at Which the Charge-Transfer Band Reaches the Baseline Value for the Charge-Transfer Salts of $[\text{Mo}_6\text{O}_{19}]^{2-}$ Acceptor with Various Me-ANT- $\text{CH}_2\text{-NR}_3^+$ Donors

| |  |  |  |  |
|-----------------------------------|---|---|---|--|
| | λ_o (nm) | λ_o (nm) | λ_o (nm) | λ_o (nm) |
| $[\text{Mo}_6\text{O}_{19}]^{2-}$ | 720 (red) | 750 (dark-red) | 750 (dark-red) | 650 (orange) |

(b) Variation of the Polyalkyl Chain Length. Changes in the length of the polyalkyl chain linking the cationic anchor to the aromatic core resulted in a significant decrease of the oxidation potential of the

arene moiety and substantial changes in the UV/vis spectra. For example, we compared two anthracene derivatives linked to pyridinium via a hydrocarbon chain of one or three methylene bridges (see Chart 1). Cocrystallization of these two donors, viz., Me-ANT-CH₂-Py⁺ and ANT-(CH₂)₃-Py⁺, with the same Keggin-type POM [SiMo₁₂O₄₀]⁴⁻ led to the formation of red-brown and dark brown crystals, respectively, of the corresponding charge-transfer salts. Accordingly, [Me-ANT-CH₂-Py⁺]₄[SiMo₁₂O₄₀]⁴⁻ showed a UV/vis spectrum with a charge-transfer absorption extending to λ_o = 800 nm, while the charge-transfer band of the analogous [ANT-(CH₂)₃-Py⁺]₄[SiMo₁₂O₄₀]⁴⁻ salt was substantially red-shifted (λ_o = 1000 nm), in accordance with a 160-mV decrease in the oxidation potential, on going from a one-methylene to a four-methylene chain. The latter salt showed a clear maximum of the charge-transfer absorption at λ_{max} = 610 nm (see Figure 3A and Table 4). Similarly, the attachment of a pyridinium anchor to a pyrene nucleus through a chain of variable length (in the PYR-CH₂-Py⁺ and PYR-(CH₂)₄-Py⁺ donors) decreased the oxidation potential of the arene by 200 mV (see Chart 1). As a consequence, the new absorption band of the [SiMo₁₂O₄₀]⁴⁻ charge-transfer salt with PYR-(CH₂)₄-Py⁺ was red-shifted by more than 100 nm as compared to that of the charge-transfer salt with PYR-CH₂-Py⁺ (see Figure 3B and Table 4).

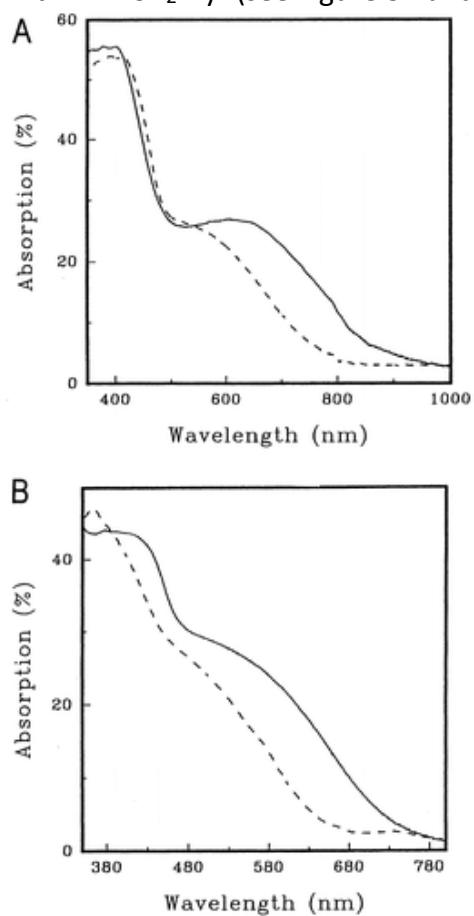
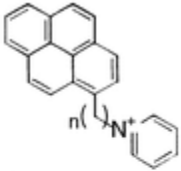
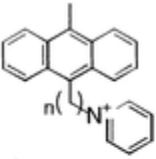


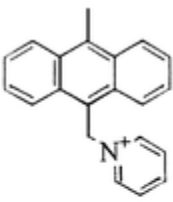
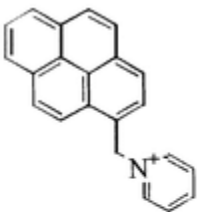
Figure 3 Diffuse reflectance spectra of the crystalline charge-transfer salts of [SiMo₁₂O₄₀]⁴⁻ acceptor with (A) ANT-(CH₂)₃-Py⁺ (—) and Me-ANT-CH₂-Py⁺ (---) and (B) PYR-(CH₂)₄-Py⁺ (—) and PYR-CH₂-Py⁺ (---).

Table 4. Wavelengths (λ_o) at Which the Charge-Transfer Band Reaches the Baseline Value for the Charge-Transfer Salts of $[\text{Mo}_6\text{O}_{19}]^{2-}$ and $[\text{SiMo}_{12}\text{O}_{40}]^{4-}$ Acceptors with Electron Donors Substituted with a Pyridinium Ring via Polyalkyl Chains of Various Lengths

| |  |  |
|--|---|--|
| | $n = 1$ λ_o (nm) | $n = 4$ λ_o (nm) |
| $[\text{Mo}_6\text{O}_{19}]^{2-}$ | 680 (orange-red) | 800 (red-brown) |
| | $n = 1$ λ_o (nm) | $n = 3$ λ_o (nm) |
| $[\text{SiMo}_{12}\text{O}_{40}]^{4-}$ | 800 (red-brown) | 1000 (dark brown) $\lambda_{\text{max}} = 610 \text{ nm}$ |

(c) Variation of the Aromatic Nucleus. We compared charge-transfer salts of the Lindqvist POM $[\text{Mo}_6\text{O}_{19}]^{2-}$ with the electron donors Me-ANT- $\text{CH}_2\text{-Py}^+$ and PYR- $\text{CH}_2\text{-Py}^+$, both of which contain pyridinium anchors with a short methylene bridge (see Chart 1). Although the oxidation potentials of these two donors differ by 110 mV, the UV/vis (diffuse reflectance) spectra of their charge-transfer salts with the same electron acceptor $[\text{Mo}_6\text{O}_{19}]^{2-}$ were very similar, with a broad charge-transfer absorption band extending to $\sim 700 \text{ nm}$ in both cases (see Table 5).

Table 5. Wavelengths (λ_o) at Which the Charge-Transfer Band Reaches the Baseline Value for the Charge-Transfer Salts of $[\text{Mo}_6\text{O}_{19}]^{2-}$ Acceptor with Two Donors of Different Aromatic Nuclei

| |  |  |
|-----------------------------------|---|---|
| | λ_o (nm) | λ_o (nm) |
| $[\text{Mo}_6\text{O}_{19}]^{2-}$ | 720 (red) | 680 (orange-red) |

(d) Two Modifications of $[\text{PYR-CH}_2\text{-NMe}_3^+]_2[\text{Mo}_6\text{O}_{19}]^{2-}$. The pyrenyl hexamolybdate crystals formed two modifications that were strongly differentiated by color. Thus, the triclinic modification formed

dark red crystals, whereas the monoclinic modification formed orange/yellow crystals. The color difference was clearly revealed in the diffuse reflectance spectra, which showed additional absorptions of the red crystals between 500 and 600 nm as well as at 850 nm (see Figure 4).

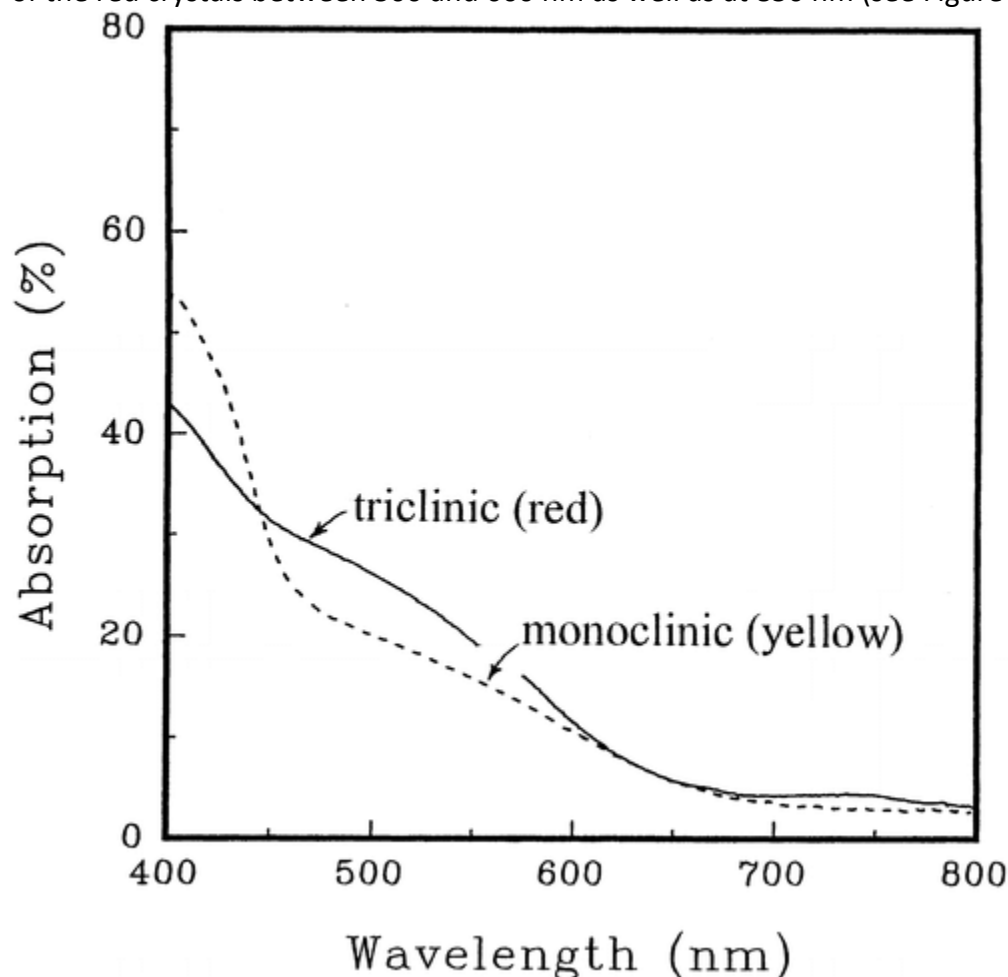


Figure 4 Diffuse reflectance spectra of the red triclinic (—) and the orange/yellow monoclinic (---) modification of the charge-transfer salt of $\text{PYR-CH}_2\text{NMe}_3^+$ donor with $[\text{Mo}_6\text{O}_{19}]^{2-}$ acceptor.

III. Structural Characterization of the Polyoxometalates Salts. 1. Structural Variations Depending on the Nature of the Cationic Anchor.

The Lindqvist-type dianion $[\text{Mo}_6\text{O}_{19}]^{2-}$, which consists of six octahedral MoO_6 units, has an isometric shape of a regular octahedron with 6 terminal oxygens at its vertexes, 12 bridging oxygens at the center of its edges, and 1 oxygen in its center. Its minimum diameter (distance between two opposite faces) is $d_{\text{min}} = 4.45 \text{ \AA}$, and its maximum diameter (distance between two opposite vertexes) is $d_{\text{max}} = 8.05 \text{ \AA}$. With the nonbonding radius of oxygen ($r = 1.52 \text{ \AA}$),¹⁵ the corresponding van der Waals dimensions are 7.50 and 11.10 \AA , respectively. In contrast, anthracene and pyrene have highly anisometric (planar) shapes, with a van der Waals thickness of about 3.40 \AA and a size of $7.4 \times 11.6 \text{ \AA}$ and $9.2 \times 11.6 \text{ \AA}$, respectively. Since the combination of such differently shaped donor and acceptor moieties within the same crystal lattice represents an

experimental challenge, we note that the role of Coulombic forces may be of primary importance because electrostatic interactions provide, in general, sufficient energy to cocrystallize such structurally incompatible molecules. Moreover, the charges of the components determine the donor/acceptor ratio (viz., 2:1 or 4:1 for the Lindqvist and the Keggin-type POMs, respectively) to satisfy electroneutrality of the cocrystals. Despite the complications due to incompatible shapes and sizes, the donor and acceptor moieties in the POM cocrystals are, in general, well organized to optimize charge-transfer interactions. For example, in the crystals containing Me-ANT-CH₂-Py⁺, the π -donor plane of the anthracene nucleus and one oxygen facet of the acceptor octahedron face each other with high degree of orbital overlap at a dihedral angle of 6° and an interplanar distance of about 3.1 Å (see Figure 5).¹⁶

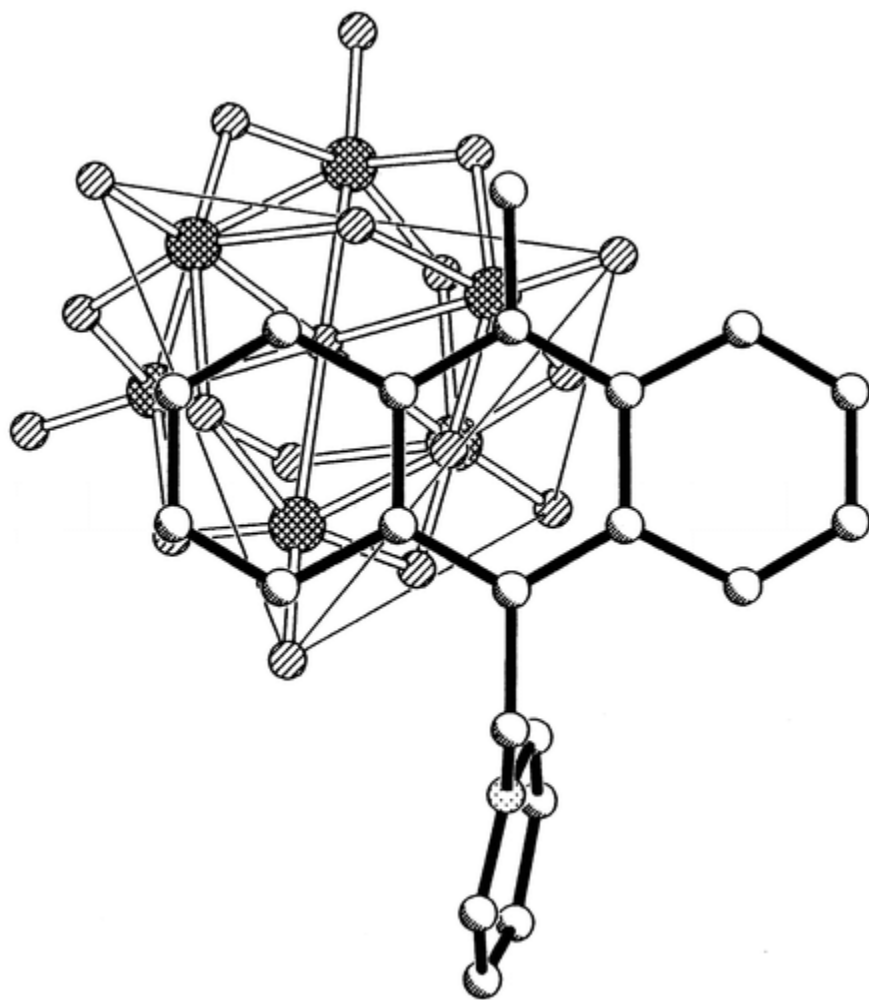


Figure 5 Overlap of the anthracene nucleus and pyridinium anchor with two octahedral surfaces of the polyoxometalate in the charge-transfer salt of Me-ANT-CH₂-Py⁺ with [Mo₆O₁₉]²⁻ acceptor.

The 2:1 donor/acceptor ratio prevents the formation of regular alternate donor/acceptor stacks, as observed in crystalline aromatic donor/acceptor complexes. Instead, a unique DAD/DAD/DAD... sequence is observed in the stacking (see Figure 6), where two neighboring donor moieties are

cofacially oriented with an interplanar distance of 3.46 Å, which allows a high degree of π -orbital overlap (see Figure 7). Such a “dimeric” packing of the aromatic donor moieties satisfies the 2:1 stoichiometry based on the ionic charges, and it also accommodates the different shapes and sizes of donor and acceptor. This is thus an important structural feature of all Lindqvist-type structures investigated in this work. The steric conditions for optimum donor/acceptor contact in the Me-ANT-CH₂-Py⁺ crystal are provided by the suitable size and shape of the cationic tether. Thus, the short methylene bridge and the flat shape of the pyridinium cause the latter to approach the oxygen face of POM that is adjacent to that overlapping with the anthracene nucleus, at a dihedral angle of 27° and an interplanar distance of 3.23 Å (see Figure 8).¹⁷

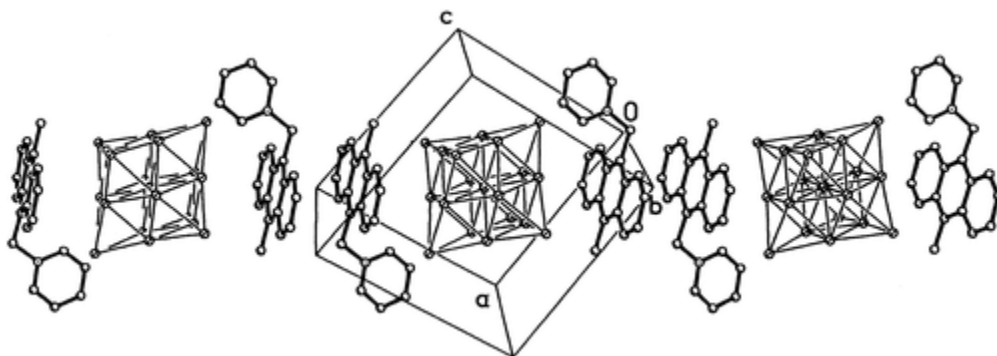


Figure 6 Infinite stacks of anthracene donor and polyoxometalate acceptor with DAD/DAD/DAD sequence in the crystal structure of (Me-ANT-CH₂-Py⁺)₂[Mo₆O₁₉]²⁻ salt.

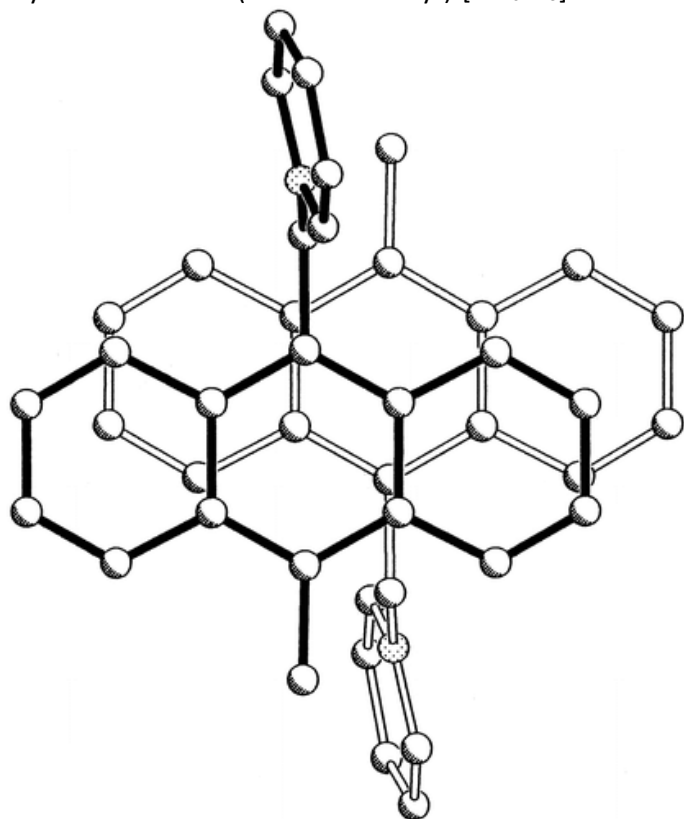


Figure 7 Overlap of “dimeric” anthracene nuclei in the crystal structure of (Me-ANT-CH₂-Py⁺)₂[Mo₆O₁₉]²⁻ salt.

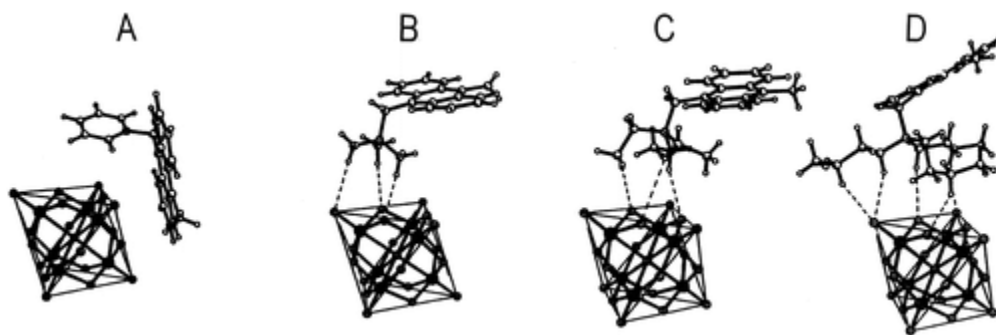


Figure 8 Orientations of anthracene donors with various anchors (A = Py^+ , B = NMe_3^+ , C = NEt_3^+ , D = NBu_3^+) relative to $[\text{Mo}_6\text{O}_{19}]^{2-}$ acceptor. The dashed lines show the short C – H \cdots O contacts.

Remarkably, the replacement of the pyridinium anchor by a trialkylammonium group dramatically changes the donor/acceptor interactions in this series of crystals. Although the positively charged nitrogen atoms remain close to the oxygen surface of the POM anion in all structures – the distances from N^+ to the nearest oxygen plane are 3.76, 4.16, and 4.19 Å for trimethyl-, triethyl-, and tributylammonium anchors, respectively – the orientation of the ammonium groups relative to the POM body effects the removal of the attached anthracene moiety away from the POM octahedral surface (see Figure 8). In other words, the structural differences are caused not by changes in the size of the anchors [the changes in the distances between the nitrogen center and the oxygen surface being rather small (within 1 Å), *vide supra*], but by changes in the chemical nature of the anchors. Thus, Figure 8 demonstrates that the orientation of the trialkylammonium anchor relative to the anionic surface is defined by an optimization of C – H \cdots O bonding interactions.¹⁸ Optimum conditions for such interactions are achieved when the trialkylammonium “umbrella” opens toward the oxygen surface, which results in a remote position of the bridging methylene groups as well as of the (tethered) anthracene moiety. Moreover, if the C – H \cdots O interactions involve most of the surface oxygen atoms, the anthracene (π -) donor moiety has little chance to approach the POM surface. In fact, all structures exhibit only “point contacts” between anthracene and POM moieties. Nevertheless, the intense colors of all crystals remind us of the significant charge-transfer interactions between anthracene and POM, even under such unfavorable conditions.¹⁹

Independent of the type of cationic anchor, a dimeric aggregation of the anthracene donors is observed in all crystals. Thus, the separation between the cofacially oriented anthracene moieties changes only slightly from 3.44 to 3.51 Å, on going from a trimethyl- to a tributylammonium anchor. The outer surfaces of the anthracene dimers are more or less ($\text{Py} < \text{NMe}_3 < \text{NEt}_3 < \text{NBu}_3$) covered by the alkyl substituents of the anchors, which limits the possibility of contacts between the arene and POM. It also limits possible contacts between two (dimeric) couples of anthracenes. Thus, the structure with trimethylammonium anchor shows the dimeric anthracene units organized in a two-dimensional layer

(see Figure 9A). Two couples of anthracenes are separated by about 3.6 Å and exhibit a dihedral angle of 23°. In contrast, the structure with the triethylammonium anchor shows one-dimensional ladder-like stacks of anthracene couples (with a separation of 3.38 Å, see Figure 9B), and the tributylammonium anchors inhibit completely any association between anthracene couples.

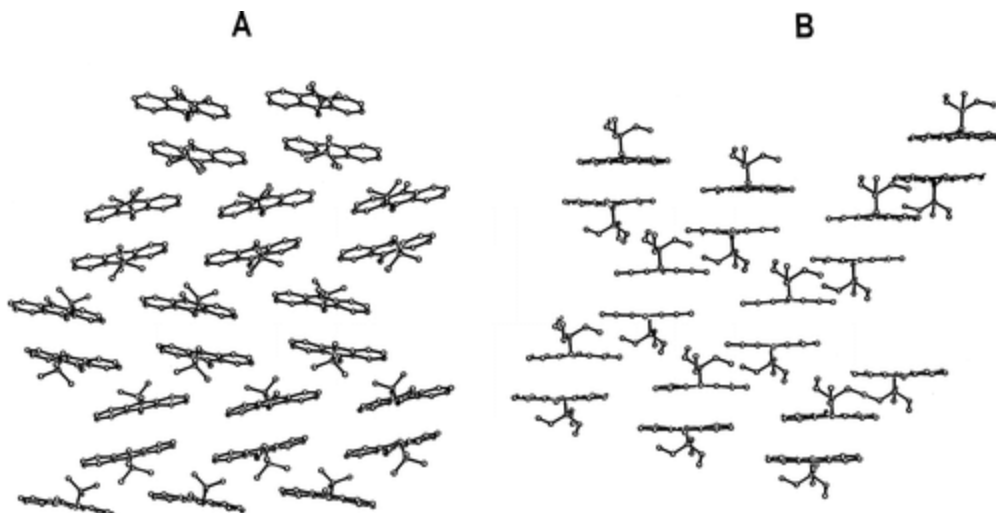


Figure 9 Arrangement of “dimeric” anthracene donors with (A) a NMe₃⁺ anchor forming two-dimensional layers and (B) a NBu₃⁺ anchor forming ladder-like one-dimensional stacks.

2. Two Polymorphic Modifications of [PYR-CH₂-NMe₃⁺]₂[Mo₆O₁₉]²⁻. Since the chemical compositions of the two polymorphic modifications of [PYR CH₂ NMe₃⁺]₂[Mo₆O₁₉]²⁻ are identical, the different colors of these two types of crystals are solely the result of different intermolecular arrangement within the crystal lattices. Thus, the comparison of the crystal structures of the two modifications provides a rare opportunity to gain insight into the relationship between crystal structure and charge-transfer interactions of POM cocrystals.

A simple comparison of the primary ionic interactions in these two crystal modifications reveals a significant difference. In the red triclinic (α) modification, the trimethylammonium anchor maintains a side contact with the POM surface that allows the pyrene moiety to come close to the adjacent oxygen surface of the POM. In contrast, the orange/yellow monoclinic (β) modification contains the trimethylammonium anchor in an “umbrella-like” orientation which moves the pyrene nucleus away from the POM body (see Figure 10). As a result, we observe a strong overlap between the POM oxygen surface and pyrene in the red modification, with an interplanar angle of only 16° and a distance of about 3.2 Å. Infinite stacks of DAD/DAD/DAD... are formed, similar to those observed with Me-ANT-CH₂-Py⁺ (compare Figure 6). In contrast, only local “point contacts” are found between the donor and acceptor moieties in the orange (β) modification.

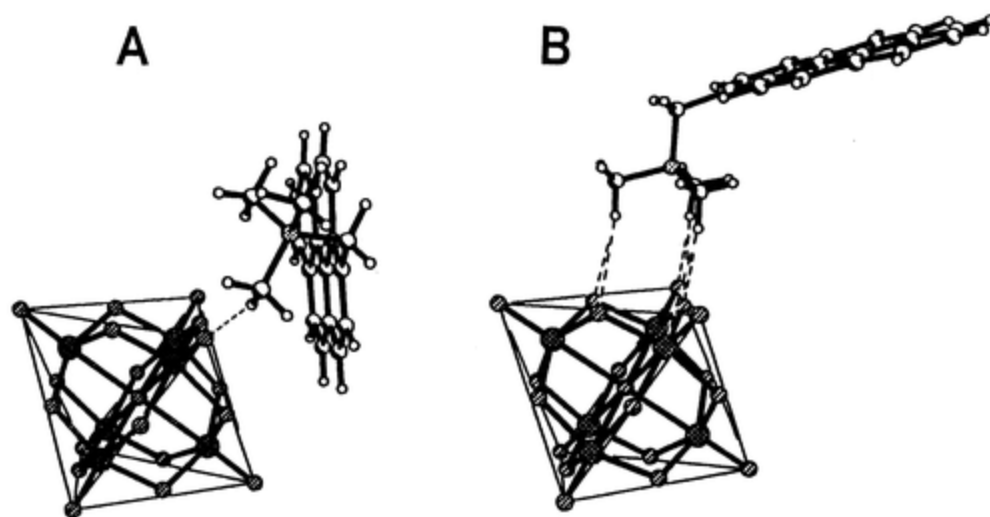


Figure 10 Relative orientation of $\text{PYR-CH}_2\text{-NMe}_3^+$ and $[\text{Mo}_6\text{O}_{19}]^{2-}$ in (A) the red triclinic and (B) the orange/yellow monoclinic modification. The dashed lines show the short $\text{C-H}\cdots\text{O}$ contacts.

Both modifications exhibit a similar (relative) orientation of the dimeric pyrenyl units with comparable interplanar distances of 3.40 and 3.48 Å for the red and the orange crystals, respectively. However, the red crystals do not show any interactions between the pyrene couples, whereas the orange modification does show interactions between pyrene dimers at a distance of about 3.86 Å. As a result, irregular stacks of pyrene units are found along the *b*-axis.

IV. Time-Resolved Diffuse Reflectance Spectroscopy. The assignment of the low-energy absorption bands to charge-transfer transitions in the diffuse reflectance spectra of the colored crystals (see section II) was substantiated by time-resolved spectroscopic measurements utilizing a picosecond laser flash photolysis apparatus in the diffuse reflectance mode (see the Experimental Section). The samples of the colored CT crystals were ground to a fine powder, diluted in a colorless KPF_6 matrix (5–10 wt %), and then photoexcited with the second harmonic output of a 25-ps Nd:YAG laser at 532 nm, where neither the POMs nor the various aromatic donors absorbed. The transient absorption spectra were recorded in the diffuse reflectance mode, and the kinetics of the transients were obtained by monitoring the absorption, viz., $\text{Abs [\%]} = 100 \times (1 - R/R_0)$, on the picosecond and early nanosecond time scales.

1. The Two Modifications of $[\text{PYR-CH}_2\text{-NMe}_3^+]_2\text{Mo}_6\text{O}_{19}^{2-}$. The two differently colored modifications of the hexamolybdate salt of trimethylammonium-substituted pyrene, viz., red triclinic and orange/yellow monoclinic crystals, show different diffuse reflectance spectra in the ground state (see Figure 4, *vide supra*). However, the *transient* diffuse reflectance spectra obtained upon 532-nm photoexcitation with a 25-ps laser pulse were very similar for both modifications. Thus, a broad absorption was observed which covered the entire wavelength range of the detector from 550 to 900 nm and was topped by a

narrow absorption band centered at 675 nm (see Figure 11). The latter absorption band was ascribed to the well-known absorption spectrum of pyrene cation radical.²⁰⁻²² The broad absorptions in the 500–600-nm range were tentatively assigned to the pyrene cation–radical π -dimer, viz., $(\text{PYR})_2^{+\bullet}$, on the basis of laser flash photolysis^{20,21} and electron pulse radiolysis²³ experiments in solution. In summary, laser excitation at 532 nm of both modifications of this charge-transfer crystal resulted in the observation of a transient spectrum that closely resembled that of pyrene cation radical in its monomeric and dimeric forms. This result was in accord with Mulliken theory,¹² which predicts one-electron transfer from the donor to the acceptor moiety upon charge-transfer excitation of donor/acceptor complexes. Most importantly, the red (triclinic) and the orange/yellow (monoclinic) crystalline samples exhibited quite different solid-state kinetics. Thus, the pyrene cation radical photogenerated in the red modification decayed about 4 times faster ($k = 1.8 \times 10^{10} \text{ s}^{-1}$) than that generated in the yellow modification ($k = 5 \times 10^9 \text{ s}^{-1}$).

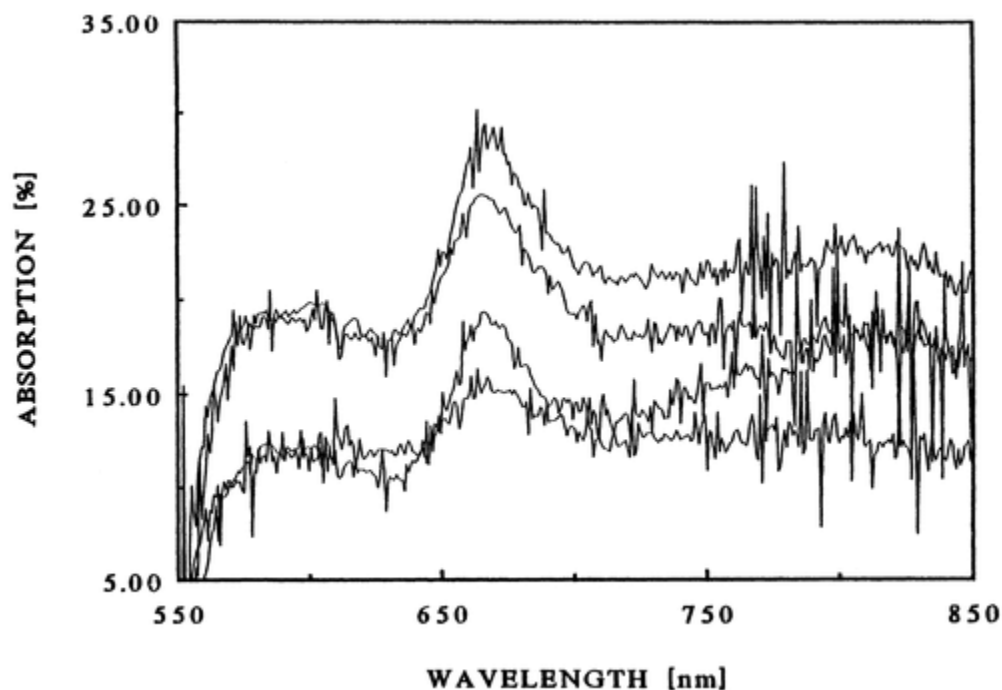


Figure 11 Transient (diffuse reflectance) spectra obtained at (top to bottom) 50, 90, 200, and 2000 ps following 25-ps laser excitation (at 532 nm) of the charge-transfer salt of $\text{PYR-CH}_2\text{-NMe}_3^+$ donor with $[\text{Mo}_6\text{O}_{19}]^{2-}$ acceptor (monoclinic modification).

2. The Hexamolybdate Salts of Trimethyl-, Triethyl-, and Tributylammonium-Substituted

Anthracenes. A comparison of the spectral and kinetic data of the hexamolybdate salts of three different trialkylammonium-substituted anthracenes revealed several unique features for the tributylammonium derivative, which were not observed with the trimethyl and triethyl analogues. First, the transient diffuse reflectance spectrum of the tributylammonium derivative showed a structured absorption band in the wavelength range from 600 to 900 nm, with distinct peaks at 726

and 795 nm (see Figure 12A). In contrast, the trimethyl- and triethylammonium-substituted anthracenes showed broad transient absorptions centered at 800 nm (see Figure 12B). Although these transient absorption spectra differed somewhat from the spectra of (isolated) anthracene cation radical (recorded in solution²⁴ or in the solid zeolite-Y matrix)²⁵ as well as the anthracene cation radical π -dimer (which exhibited a slightly broadened band at 726 nm and an additional broad absorption centered at 600 nm in solution),²⁴ we tentatively assigned these transient absorptions to the charge-transfer exciton state of these charge-transfer crystals.

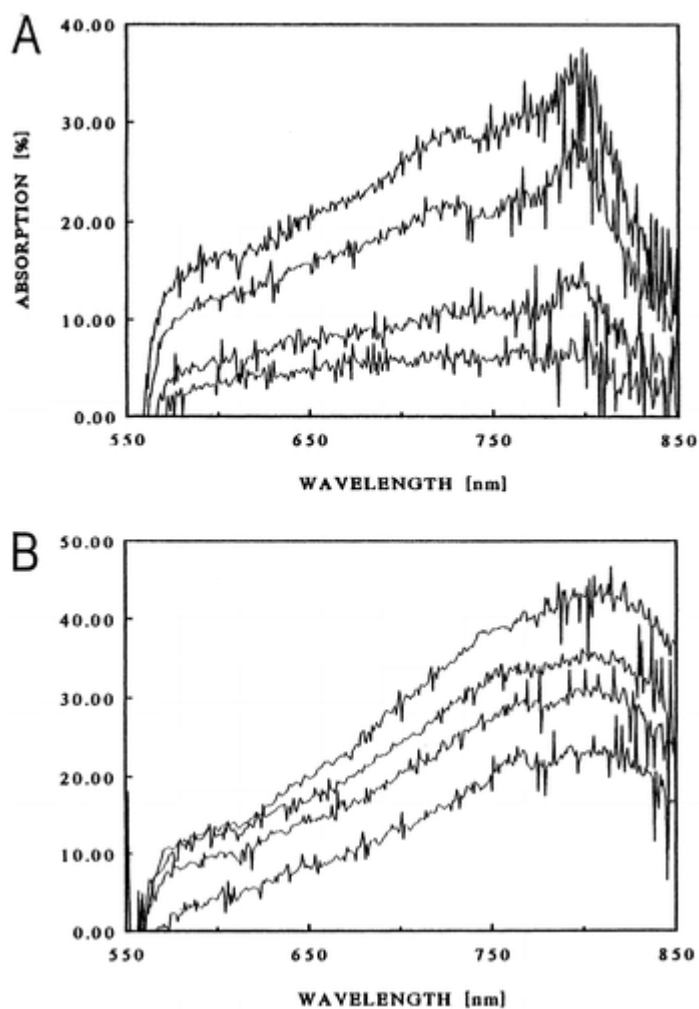
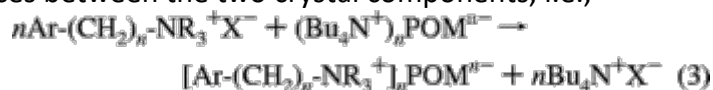


Figure 12 Transient (diffuse reflectance) spectra obtained at (top to bottom) 50, 100, 200, and 500 ps following 25-ps laser excitation (at 532 nm) of the charge-transfer salts of (A) ANT-CH₂-NBu₃⁺ donor and (B) ANT-CH₂-NMe₃⁺ donor with [Mo₆O₁₉]²⁻ acceptor.

Most importantly, the transient diffuse reflectance spectrum of tributylammonium-substituted anthracene showed a decay kinetics very different from those of the trimethyl- and triethyl-substituted analogues. Thus, the tributyl-substituted derivative exhibited a clean monoexponential decay of the transient spectrum with a rate constant of $k = 5 \times 10^9 \text{ s}^{-1}$, whereas the trimethyl- and triethyl-substituted analogues showed biphasic decay kinetics with $k_{\text{fast}} \approx 1.6 \times 10^{10} \text{ s}^{-1}$ and $k_{\text{slow}} \approx 1.7 \times 10^8 \text{ s}^{-1}$.

Discussion

Efficient cocrystallization of spherical (Lindqvist-type and Keggin-type) POM acceptors and planar aromatic donors is readily achieved by attaching a cationic anchor onto the arene moiety, which results in strong Coulombic forces between the two crystal components, i.e.,



where Ar = 10-methylanthracen-9-yl or pyren-1-yl, $\text{NR}_3^+ = \text{Py}^+, \text{NMe}_3^+, \text{NEt}_3^+, \text{or NBU}_3^+, n = 1, 3, \text{ or } 4,$ and $\text{X}^- = \text{I}^- \text{ or } \text{CF}_3\text{SO}_3^-$. As a result, intensely colored crystals are obtained which represent new charge-transfer materials.

Whereas the starting materials are colorless or yellow, the new salts exhibit characteristic bright colors from yellow/orange to dark red/brown, depending on the POM/arene combination. Accordingly, the (diffuse reflectance) UV/vis spectra of the crystals show additional broad absorption bands that are not present in the spectrum of either the arene cations or the POM anions, and these new absorptions are ascribed to *charge-transfer* transitions. The charge-transfer interactions are inherent to the crystalline state only since the intense colors are invariably bleached when the crystals are redissolved in strong polar solvents such as dimethylformamide or dimethyl sulfoxide. Since these solvents are known to break up ionic aggregates,^{26,27} the colors of the crystalline salts result from electronic interactions of the cations and the anions in the crystal lattice.

The electrostatic binding of the trialkylammonium or pyridinium anchor to the anionic surface of the POM represents the primary interaction between POM and arene which brings the arene moiety in close proximity to the POM surface and allows charge-transfer interactions to develop. The assignment of the intense colors to charge-transfer transitions is confirmed by the progressive bathochromic shift of the new absorption bands of the various complexes in Figures 1–3 with increasing acceptor strength (E°_{red}) of the POM from $[\text{W}_6\text{O}_{19}]^{2-}$ to $[\text{Mo}_6\text{O}_{19}]^{2-}$ and from $[\text{SiW}_{12}\text{O}_{40}]^{4-}$ to $[\text{SiMo}_{12}\text{O}_{40}]^{4-}$. Such a correlation between spectral shifts and acceptor strength in isostructural donor/acceptor complexes is predicted by Mulliken theory¹² as depicted in eq 4,

$$h\nu_{\text{CT}} = a[E^\circ_{\text{ox}}(\text{D}) - E^\circ_{\text{red}}(\text{A})] + \text{const} \quad (4)$$

where $h\nu_{\text{CT}}$ is the transition energy of the charge-transfer absorption band, $E^\circ_{\text{ox}}(\text{D})$ is the oxidation potential of the aromatic donors, $E^\circ_{\text{red}}(\text{A})$ is the reduction potential of the POMs, and $0 < a < 1$.

However, the position of the charge-transfer absorptions is determined not only by the oxidation and reduction potentials of arene and POM, respectively, but also by the distance and relative orientation of donor and acceptor in the crystal lattice.¹⁹ This is best demonstrated with the two modifications of the $[\text{PYR}-\text{CH}_2-\text{NMe}_3^+]_2[\text{Mo}_6\text{O}_{19}]^{2-}$ salt. Thus, the difference in color between the red triclinic and the

orange/yellow monoclinic modification (see Figure 4) results from different types of contacts between the pyrene moiety and the POM surface in the two modifications (see Figure 10). Thus, in the triclinic modification, the pyrene nucleus is cofacially oriented relative to the oxygen surface of the hexamolybdate moiety, which leads to a strong orbital overlap between donor and acceptor. As a result, strong charge-transfer interactions are observed, as evidenced by a red shift in the CT absorption band as compared to the band for the monoclinic modification.

The charge-transfer character of the intense colors of the crystals as well as the new absorptions in the visible wavelength region is further confirmed by the time-resolved absorption measurements upon laser excitation of the crystals. In general, all laser experiments result in the observation of transient absorption spectra that closely resemble those of the corresponding arene cation radicals in monomeric or (π -) dimeric form. Thus, transient spectra similar to those of anthracene or pyrene cation radical and their corresponding (π -) dimers are obtained. Mulliken theory¹² predicts that photoexcitation of charge-transfer transitions effects the transfer of an electron from the donor to the acceptor moiety in the donor/acceptor complex, which results in the formation of cation and anion radical,s as observed in our laser experiments.²⁸

Moreover, the decay kinetics of the excited charge-transfer state (due to back-electron transfer) obtained from time-resolved absorption measurements on the picosecond/nanosecond time scales provides additional information on the strength of the charge-transfer interaction. Thus, the stronger the charge-transfer interaction, the weaker is the driving force for back-electron transfer following the photoinduced charge separation process. Since Marcus theory²⁹ predicts increasing rate constants for back-electron transfer with decreasing driving force (“inverted” free energy correlation), increased back-electron-transfer rates reveal strong charge-transfer interactions. The laser experiments with the triclinic and monoclinic modification of the pyrene/POM crystals are consistent with this correlation. Thus, the red modification with close donor/acceptor contacts and strong charge-transfer character exhibits a much shorter-lived excited state ($k = 1.8 \times 10^{10} \text{ s}^{-1}$) than that of the monoclinic, orange/yellow modification with greater donor/acceptor distances and weaker charge-transfer interactions ($k = 5 \times 10^9 \text{ s}^{-1}$).

The series of CT crystals with differently substituted trialkylammonium anchors represents another case with which to study the correlation between crystal structure and charge-transfer properties by a thorough comparison of crystallographic and spectroscopic data. First, we observe similar (dark red) charge-transfer colors for the trimethyl- and the triethylammonium derivatives, whereas the CT crystals of the tributylammonium derivative are orange in color, which indicates weaker CT interactions as compared to the trimethyl- and triethylammonium analogues. Analysis of the crystal structures of all three CT crystals (see Figure 8) readily explains the weaker charge-transfer properties

in the latter case. Thus, the tributylammonium anchor is oriented in such a way that it (i) covers the entire polyoxometalate surface with its alkyl groups and (b) turns the anthracene donor away from the POM surface. Both structural features effect a substantial weakening of the charge-transfer interactions between anthracene and POM as compared to the case in crystals with trimethyl- or triethylammonium anchors.

Moreover, the transient decay kinetics of the tributylammonium derivative is very different from those of the trimethyl- and the triethylammonium analogues. First, the rate constant for back-electron transfer of $k = 5 \times 10^9 \text{ s}^{-1}$ observed with the tributylammonium anchor is one-third that obtained with the trimethyl- or triethylammonium anchor ($k = 1.6 \times 10^{10} \text{ s}^{-1}$). Second, the clean monoexponential decay that is observed only with the tributylammonium anchor is clearly related to the fact that the anthracene dimers are isolated units in this CT crystal, whereas the crystal lattices with the trimethyl- and triethylammonium anchors exhibit significant electronic interactions along the anthracene dimer stacks, which cause the nonexponential decays.

In summary, the combination of X-ray crystallographic and spectroscopic techniques applied in this work reveals a logical correlation between structure and electronic properties in various novel charge-transfer materials. Thus, the cocrystallization of a variety of spherical POM acceptors and planar arene donors with the aid of cationic anchors results in a series of charge-transfer materials which differ in structure, color, and electron-transfer kinetics. The variability of these parameters and the unique structure exhibiting dimeric donor units make these materials interesting candidates for nonlinear optical and/or ferromagnetic properties.

Experimental Section

Materials. Dichloromethane (Mallinckrodt analytical reagent) was repeatedly stirred with fresh aliquots of concentrated sulfuric acid (~20 vol %) until the acid layer remained colorless. After separation, the acid layer was washed successively with water, aqueous sodium bicarbonate, water, and aqueous sodium chloride and dried over anhydrous calcium chloride. The dichloromethane was distilled twice from P_2O_5 under an argon atmosphere and stored in a Schlenk flask equipped with a Teflon valve fitted with Viton O-rings. The tetrahydrofuran was distilled from P_2O_5 under an argon atmosphere and then refluxed over calcium hydride (~12 h). After distillation from CaH_2 , the solvents were stored in Schlenk flasks under an argon atmosphere.

Various trialkylammonium and pyridinium salts of anthracenyl and pyrenyl donors were obtained from the reaction of 9-methyl-10-chloromethylantracene with the corresponding trialkylamine (or pyridine) in tetrahydrofuran at 0 °C and purified by repeated crystallization from acetonitrile. The trimethylene derivative $\text{ANT}-(\text{CH}_2)_3\text{Py}^+$ was prepared from the reaction of 3-(9-

anthryl)bromopropane³⁰ with pyridine in refluxing tetrahydrofuran, and the resulting colorless precipitate was purified by recrystallization from acetonitrile: mp > 300 °C (dec); ¹H NMR (CDCl₃) δ 2.41 (m, 2 H), 3.62 (t, 2 H), 3.80 (t, 2 H), 7.51–8.32 (m, 13 H), 8.38 (s, 1 H). Similarly, the tetramethylene derivative PYR-(CH₂)₄Py⁺ was obtained by the reaction of 4-(1-pyrenyl)bromobutane (prepared from 1-pyrenebutyric acid by lithium aluminum hydride reduction followed by treatment with PBr₃ using standard procedures): mp > 370 °C (dec); ¹H NMR (CDCl₃) δ 2.03 (m, 2 H), 3.36 (t, 2 H), 3.47 (t, 2 H), 7.85–8.30 (m, 13 H).

Preparation of the Tetrabutylammonium Salts of the Polyoxometalates. The syntheses of the tetrabutylammonium salts of the hexamolybdate³¹ (Bu₄N⁺)₂[Mo₆O₁₉]²⁻ and the hexatungstate³²(Bu₄N⁺)₂[W₆O₁₉]²⁻ have been described previously. The tetrabutylammonium salts of the silicomolybdate (Bu₄N⁺)₄[SiMo₁₂O₄₀]⁴⁻ and silicotungstate (Bu₄N⁺)₄[SiW₁₂O₄₀]⁴⁻ have been prepared from the corresponding acids by direct metathesis with tetrabutylammonium bromide, Bu₄N⁺Br⁻. Thus, 10 g (3.5 mM) of silicotungstic acid, H₄SiW₁₂O₄₀, was dissolved in small volumes of water (to obtain a close to saturated solution), and 2 g (14.5 mM) of Bu₄N⁺Br⁻ was added. The white precipitate that was formed upon stirring was filtered, rinsed with two portions (10 mL) of warm water and two portions (10 mL) of ethanol, and finally dried in an air stream. The resulting white solid was dissolved in dimethylformamide, and after a few days of slow evaporation of the solvent at 20 °C, colorless crystals of (Bu₄N⁺)₄[SiW₁₂O₄₀]⁴⁻ salt were collected. According to the same procedure, yellow crystals of (Bu₄N⁺)₄[SiMo₁₂O₄₀]⁴⁻ salt were obtained.³³

Preparation of the Charge-Transfer Crystals. Typically, a 2 mM concentration of the donor (as iodide or trifluoromethanesulfonate salt) and a 1 mM concentration of the tetrabutylammonium salt of the Lindqvist-type POM [Mo₆O₁₉]²⁻ or [W₆O₁₉]²⁻ were dissolved in 100 mL of acetonitrile. The yellow solution was stirred for several minutes, and then the solvent was slowly evaporated at 20 °C. Within 24 h, colored crystals suitable for X-ray crystallography analysis formed in the yellow solution. According to the same procedure, charge-transfer crystals of the Keggin-type POMs [SiMo₁₂O₄₀]⁴⁻ and [SiW₁₂O₄₀]⁴⁻ were obtained from a mixture of the organic donors with the POM acceptors in a 4:1 ratio in dimethyl sulfoxide. Specifically, the various charge-transfer complexes were isolated as crystalline salts and subjected to elemental analysis as follows.

(Me-ANT-CH₂-Py⁺)₂Mo₆O₁₉²⁻. Anal. Calcd for C₄₂H₃₆Mo₆N₂O₁₉: C, 34.83; H, 2.51; N, 1.93. Found: C, 34.99; H, 2.50; N, 2.02.

(Me-ANT-CH₂-Py⁺)₂W₆O₁₉²⁻. Anal. Calcd for C₄₂H₃₆N₂O₁₉W₆: C, 25.53; H, 1.84; N, 1.42. Found: C, 25.68; H, 1.93; N, 1.52.

(Me-ANT-CH₂-NEt₃⁺)₂Mo₆O₁₉²⁻. Anal. Calcd for C₄₄H₅₆Mo₆N₂O₁₉: C, 35.41; H, 3.78; N, 1.88. Found: C, 35.58; H, 3.75; N, 1.94.

(Me-ANT-CH₂-NBu₃⁺)₂Mo₆O₁₉²⁻. Anal. Calcd for C₅₆H₈₀Mo₆N₂O₁₉: C, 40.50; H, 4.86; N, 1.69. Found: C, 40.41; H, 5.00; N, 1.79.

[PYR-(CH₂)₄-Py⁺]₂Mo₆O₁₉²⁻. Anal. Calcd for C₅₀H₄₄Mo₆N₂O₁₉: C, 38.86; H, 2.86; N, 1.80. Found: C, 38.91; H, 2.87; N, 1.89.

[ANT-(CH₂)₃-Py⁺]₄SiMo₁₂O₄₀²⁻. Anal. Calcd for C₈₈H₈₀Mo₁₂N₄O₄₀Si: C, 35.08; H, 2.68; N, 1.86. Found: C, 34.86; H, 2.93; N, 1.91.³⁴

X-ray Crystallography. The intensity data for all compounds were collected with the aid of a Siemens SMART diffractometer equipped with a CCD detector using Mo K α radiation ($\lambda = 0.71073 \text{ \AA}$), at $-150 \text{ }^\circ\text{C}$, unless stated otherwise. The structures were solved by direct methods³⁵ and refined by the full matrix least-squares procedure using IBM Pentium and SGI O₂ computers (Table 6). Details of the X-ray structures of the various CT crystals are on deposit at the Cambridge Crystallographic Data Center, U.K.

Table 6. Crystallographic Parameters and Refinement Details for the Charge-Transfer

Polyoxomolybdates

| charge-transfer complex | Me-ANT-CH ₂ -Py ⁺ hexamolybdate | Me-ANT-CH ₂ -NMe ₃ ⁺ hexamolybdate | Me-ANT-CH ₂ -NEt ₃ ⁺ hexamolybdate | Me-ANT-CH ₂ -NBu ₃ ⁺ hexamolybdate | PYR-CH ₂ -NMe ₃ ⁺ hexamolybdate (red) | PYR-CH ₂ -NMe ₃ ⁺ hexamolybdate (yellow) | Me-ANT-CH ₂ -Py ⁺ silicomolybdate |
|---|--|--|--|--|--|--|--|
| Brutto formula | (C ₂₁ H ₁₈ N ⁺) ₂ Mo ₆ O ₁₉ ²⁻ | (C ₁₉ H ₂₂ N ⁺) ₂ Mo ₆ O ₁₉ ²⁻ | (C ₂₂ H ₂₈ N ⁺) ₂ Mo ₆ O ₁₉ ²⁻ | (C ₂₈ H ₄₀ N ⁺) ₂ Mo ₆ O ₁₉ ²⁻ | (C ₂₀ H ₂₀ N ⁺) ₂ Mo ₆ O ₁₉ ²⁻ | (C ₂₀ H ₂₀ N ⁺) ₂ Mo ₆ O ₁₉ ²⁻ | (C ₂₁ H ₁₈ N ⁺) ₄ SiMo ₁₂ O ₄₀ ⁴⁻ ·4C ₂ H ₆ OS |
| MW | 1448.44 | 1408.39 | 1492.55 | 1660.86 | 1428.38 | 1428.38 | 3269.34 |
| crystal symmetry | triclinic | monoclinic | triclinic | triclinic | triclinic | monoclinic | triclinic |
| space group | <i>P</i> 1 | <i>P</i> 2 ₁ / <i>c</i> | <i>P</i> 1 | <i>P</i> 1 | <i>P</i> 1 | <i>C</i> 2/ <i>c</i> | <i>P</i> 1 |
| temp (°C) | -50 | -150 | -150 | -150 | -150 | -150 | -150 |
| <i>a</i> (Å) | 10.439(1) | 13.0374(4) | 10.0083(2) | 11.7250(4) | 10.0919(6) | 33.168(1) | 12.8830(5) |
| <i>b</i> (Å) | 10.515(1) | 10.5791(3) | 10.2022(2) | 14.4431(4) | 10.2280(6) | 8.8338(3) | 15.5389(6) |
| <i>c</i> (Å) | 11.654(2) | 15.9227(5) | 13.5023(3) | 19.0626(6) | 12.4426(7) | 15.1950(5) | 15.5948(7) |
| α (deg) | 67.62(1) | 90 | 89.318(1) | 91.936(1) | 76.979(1) | 90 | 118.629(1) |
| β (deg) | 72.88(1) | 90.541(1) | 87.093(1) | 96.722(1) | 66.539(1) | 102.522(1) | 100.957(1) |
| γ (deg) | 65.21(1) | 90 | 63.959(1) | 108.205(1) | 66.532(1) | 90 | 99.159(1) |
| <i>D</i> _c (g cm ⁻³) | 2.270 | 2.130 | 2.004 | 1.816 | 2.202 | 2.183 | 2.109 |
| <i>V</i> (Å ³) | 1060.0(1) | 2196.0(1) | 1237.0(1) | 3037.0(2) | 1077.3(1) | 4346.2(2) | 2574.3(2) |
| <i>Z</i> | 1 | 2 | 1 | 2 | 1 | 4 | 1 |

| | | | | | | | |
|-----------------------------|--------------|--------------|--------------|--------------|--------------|--------------|--------------|
| total no. of reflections | 4653 | 30 466 | 14 073 | 45 249 | 21 805 | 41 441 | 25 594 |
| no. of unique reflections | 4653 | 9395 | 9392 | 26 469 | 9215 | 9603 | 20 567 |
| no. of observed reflections | 4218 | 7923 | 8687 | 16 064 | 8167 | 7473 | 14 331 |
| intensity threshold | $3\sigma(I)$ | $2\sigma(I)$ | $2\sigma(I)$ | $2\sigma(I)$ | $2\sigma(I)$ | $2\sigma(I)$ | $2\sigma(I)$ |
| R_1 | 0.016 | 0.0224 | 0.0262 | 0.0736 | 0.0218 | 0.0211 | 0.0940 |
| wR_2 | 0.019 | 0.0543 | 0.0652 | 0.1119 | 0.0565 | 0.0500 | 0.1710 |

Time-Resolved Diffuse Reflectance Spectroscopy. The diffuse reflectance laser photolysis setup has been described previously in detail.²⁵ Briefly, the second-harmonic output (532 nm, 25 ps) of a mode-locked Nd:YAG laser (Quantel, YG 501-C) was used as the excitation source. The fundamental laser pulse (1064 nm) was focused into a 10-cm quartz cuvette containing a 1:1 mixture of H₂O and D₂O to generate a white continuum pulse of 25-ps duration, which was utilized as the analyzing light pulse. The continuum light was split into two beams, which were used as reference light and probe light for the powder sample which was stored in a 1-mm cuvette. The diffuse-reflected probe light was collected by fiber optics and detected by an unintensified dual-diode-array detector (Princeton Instruments) attached to a flat-field spectrograph (Instruments S.A.). The diffuse reflectance transient absorption spectra, which represent an average of 100–300 laser shots, are presented as percentage absorption, viz., % ABS = $100 \times (1 - R/R_0)$, with R and R_0 representing the diffuse-reflected sample light and the reference light, respectively.

Acknowledgment

We thank the National Science Foundation and the Robert A. Welch Foundation for financial support. We thank J. D. Korp for the crystal structure analysis of the anthracenylpyridinium hexamolybdate at -50 °C, and R. Rathore for providing the precursor ammonium salts and helpful (synthetic) suggestions to us as well as contributing to many fruitful discussions.

References

- ¹Hill, C. L., Ed. Polyoxometalates. *Chem. Rev.* **1998**, *98* (1, Thematic Issue).
- ²(a) Dabbabi, M.; Boyer, M.; Launay, J. P.; Jeannin, Y. *Electroanal. Chem.* **1977**, *76*, 153. (b) Pope, M. T.; Varga, J. M. *Inorg. Chem.* **1966**, *7*, 1249. (c) Launay, J. P. *J. Inorg. Nucl. Chem.* **1976**, *18*, 807.
- ³For reviews on the chemistry, the properties, and the applications of polyoxometalates, see: (a) Pope, M. T. *Heteropoly and Isopoly Oxometalates*; Springer-Verlag: Berlin, 1983. (b) Pope, M. T.; Müller, A. *Angew. Chem., Int. Ed. Engl.* **1991**, *30*, 34. (c) *Polyoxometalates: from Platonic Solids to Anti-retroviral Activity*; Pope, M. T., Müller, A., Eds.; Kluwer Academic Publishers: Norwell, MA, 1994. (d) Ma, J. C.; Dougherty, D. A. *Chem. Rev.* **1997**, *97*, 1303.

- ⁴(a) Prosser-McCartha, C. M.; Kadkhodayan, M.; Williamson, M. M.; Bouchard, D. A.; Hill, C. L. *J. Chem. Soc., Chem. Commun.* **1986**, 1747. (b) Williamson, M. M.; Bouchard, D. A.; Hill, C. L. *Inorg. Chem.* **1987**, *26*, 1436. (c) Hill, C. L.; Bouchard, D. A.; Kadkhodayan, M.; Williamson, M. M.; Schmidt, J. A.; Hilinski, E. F. *J. Am. Chem. Soc.* **1988**, *110*, 5471. (d) Niu, J. Y.; You, X. Z.; Duan, C. Y.; Fun, H. K.; Zhou, Z. Y. *Inorg. Chem.* **1996**, *35*, 4211.
- ⁵(a) Attanasio, D.; Bonamico, M.; Fares, V.; Imperatori, P.; Suber, L. *J. Chem. Soc., Dalton Trans.* **1990**, 3221. (b) Zhang, X.-M.; Shan, B.-Z.; Bai, Z.-P.; You, X.-Z.; Duan, C.-Y. *Chem. Mater.* **1997**, *9*, 2687.
- ⁶(a) Ouahab, L. *Chem. Mater.* **1997**, *9*, 1909 and references therein. (b) Le Maguerès, P.; Ouahab, L.; Golhen, S.; Grandjean, D.; Pena, O.; Jégaden, J. C.; Gómez-García, C. J.; Delhaès, P. *Inorg. Chem.* **1994**, *33*, 5180. (c) Attanasio, D.; Bellito, C.; Bonamico, M.; Righini, G.; Staulo, G. *Mater. Res. Soc., Symp. Proc.* **1992**, *247*, 205.
- ⁷For other examples of cocrystallizations of spherical (fullerene) and planar (porphyrin) molecules, see: Olmstead, M. M.; Costa, D. A.; Maitra, K.; Noll, B. C.; Phillips, S. L.; Van Calcar, P. M.; Balch, A. *J. Am. Chem. Soc.* **1999**, *121*, 7090.
- ⁸Veya, P. L.; Kochi, J. K. *J. Organomet. Chem.* **1995**, *488*, C4–C8.
- ⁹(a) Lindqvist, I. *Ark. Kemi.* **1953**, *5*, 247. (b) Keggin, J. F. *Proc. R. Soc. London Ser. A* **1934**, *144*, 75.
- ¹⁰The polyoxometalate charge-transfer salts were insoluble in less polar media such as tetrahydrofuran, diethyl ether, various hydrocarbons, or dichloromethane.
- ¹¹Note that even upon addition of extremely large (excess) amounts of the organic donor to a solution containing the polyoxometalate acceptor, solely the absorption bands of the two components were detected by UV/vis spectroscopy.
- ¹²(a) Mulliken, R. S. *J. Am. Chem. Soc.* **1952**, *74*, 811. (b) Mulliken, R. S.; Person, W. B. *Molecular Complexes. A Lecture and Reprint Volume*; Wiley: New York, 1969. (c) Foster, R. *Organic Charge-Transfer Complexes*; Academic: New York, 1969.
- ¹³Vogler, A.; Kunkely, H. *Top. Curr. Chem.* **1990**, *158*, 1.
- ¹⁴Note that the attachment of a pyridinium or a trialkylammonium substituent to the aromatic nucleus through a methylene chain did not affect the oxidation potential of the arene donor, and thus the only changing parameter was the bulkiness of the trialkylammonium group.
- ¹⁵Bondi, A. *J. Phys. Chem.* **1964**, *68*, 441.
- ¹⁶The sum of the van der Waals radii of carbon and oxygen is 3.22 Å.
- ¹⁷This is the perpendicular distance from the nitrogen center to the oxygen plane.
- ¹⁸Polarization of C–H bonds in the alkyl groups due to inductive effects from the quaternary nitrogen center activates such hydrogen bonding.
- ¹⁹For a detailed discussion of the distance dependence of charge-transfer interactions, see: Rathore, R.; Lindeman, S. V.; Kochi, J. K. *J. Am. Chem. Soc.* **1997**, *119*, 9393.
- ²⁰Kira, A.; Arai, S.; Imamura, M. *J. Chem. Phys.* **1971**, *54*, 4890.
- ²¹Tsuchida, A.; Tsujii, Y.; Ohoka, M.; Yamamoto, M. *J. Phys. Chem.* **1991**, *95*, 5797.
- ²²Shida, T. *Electronic Absorption Spectra of Radical Ions*; Elsevier: New York, 1988.
- ²³Rodgers, M. A. *J. Chem. Phys. Lett.* **1971**, *9*, 107.
- ²⁴Masnovi, J. M.; Kochi, J. K.; Hilinski, E. F.; Rentzepis, P. M. *J. Phys. Chem.* **1985**, *89*, 5387.
- ²⁵Yoon, K. B.; Hubig, S. M.; Kochi, J. K. *J. Phys. Chem.* **1994**, *98*, 3865.
- ²⁶(a) Bockman, T. M.; Kochi, J. K. *J. Am. Chem. Soc.* **1989**, *111*, 4669. (b) Bockman, T. M.; Kochi, J. K. *Adv. Organomet. Chem.* **1991**, *33*, 52.

- ²⁷(a) Edgell, W. F. In *Ions and Ion Pairs in Organic Reactions*; Szwarc, M., Ed.; Wiley: New York, 1972; Vol. 1, p 153 ff. (b) Masnovi, J. M.; Kochi, J. K. *J. Am. Chem. Soc.* **1985**, *107*, 7880. (c) Kosower, E. M.; Skorcz, J. A. *J. Am. Chem. Soc.* **1960**, *82*, 2195.
- ²⁸The corresponding reduced polyoxometalate (anion radical) moieties could not be detected spectroscopically since their weak absorption bands were covered by the strong absorption bands of anthracene and pyrene cation radicals and their π -dimers. See ref 8.
- ²⁹(a) Marcus, R. A. *J. Chem. Phys.* **1956**, *24*, 966. (b) Marcus, R. A. *Angew. Chem., Int. Ed. Engl.* **1993**, *32*, 1111 and references therein.
- ³⁰Leardini, R.; Nanni, D.; Pedulli, G. F.; Tundo, A.; Zanardi, G.; Foresti, E.; Palmieri, P. *J. Am. Chem. Soc.* **1989**, *111*, 7723.
- ³¹Che, M.; Fournier, M.; Launay, J. P. *J. Chem. Phys.* **1979**, *71*, 1954.
- ³²Sanchez, C.; Livage, J.; Launay, J. P.; Fournier, M. *J. Am. Chem. Soc.* **1983**, *105*, 6817.
- ³³The preparations of these ammonium salts were carried out by R. Rathore, the details to be reported separately at a later time.
- ³⁴Microanalyses by Atlantic Microlab, Inc. Norcross, GA 30091.
- ³⁵Sheldrick, G. M. *SHELXS-86, Program for Structure Solution*; University of Göttingen: Germany, 1986.